Singularities in polarization resolved angular patterns: transmittance of nematic liquid crystal cells

2007 J. Phys.: Condens. Matter 19 246102

(http://iopscience.iop.org/0953-8984/19/24/246102)

IOP PUBLISHING JOURNAL OF PHYSICS: CONDENSED MATTER

J. Phys.: Condens. Matter **19** (2007) 246102 (20pp) doi:10.1088/0953-8984/19/24/246102

Singularities in polarization resolved angular patterns: transmittance of nematic liquid crystal cells

Alexei D Kiselev

Institute of Physics, National Academy of Sciences of Ukraine, prospekt Nauki 46, 03028 Kyïv, Ukraine

E-mail: kisel@mail.cn.ua and kiselev@iop.kiev.ua

Received 12 February 2007, in final form 13 April 2007
Published 9 May 2007
Online at stacks.iop.org/JPhysCM/19/246102

Abstract

We study the angular structure of polarization of light transmitted through a nematic liquid crystal (NLC) cell by theoretically analysing the polarization state as a function of the incidence angles. For a uniformly aligned NLC cell, the 4×4 matrix formalism and the orthogonality relations are used to derive the exact expressions for the transmission and reflection matrices. The polarization resolved angular patterns in the two-dimensional projection plane are characterized in terms of the polarization singularities such as C-points (points of circular polarization) and L-lines (lines of linear polarization). For linearly polarized plane waves incident on the homeotropically aligned cell, we present the results of detailed theoretical analysis describing the structure of the polarization singularities. We apply the theory to compute the polarization patterns for various orientational structures in the NLC cell and discuss the effects induced by director orientation and biaxiality.

(Some figures in this article are in colour only in the electronic version)

1. Introduction

The optical properties of nematic liquid crystals (NLCs) have long been known to play a key part in a wide variety of liquid crystal devices [1–3]. Typically, NLCs are used as optically anisotropic materials, where the anisotropy is determined by the orientational structure, which is sensitive to external fields and, in restricted geometries, can also be influenced by changing the boundary conditions.

Similar to other anisotropic materials, the polarization state of light propagating through a liquid crystal varies due to the presence of the anisotropy. When the NLC cell is placed between two crossed polarizers, these anisotropy induced changes of the polarization manifest themselves in variations of the intensity of the transmitted light. This effect underlines the vast majority of experimental techniques devised to characterize orientational structures in NLC cells.

For example, the crystal rotation technique [4] relies on analysing the angle dependence of the transmittance of NLC cells placed between crossed polarizers. It can be regarded as a special case dealing with a one-dimensional cross-section of the conoscopic pattern.

Nowadays, conoscopy has been proved to be a useful tool for studying liquid crystal systems. It is used to detect biaxiality of NLCs [5, 6] and to measure the pretilt angle in uniaxial liquid crystal cells [7, 8]. Orientational structures and helix unwinding processes in ferroelectric smectic liquid crystals were also studied by conoscopy in [9, 10]. The conoscopic patterns of hybrid NLC cells were investigated in [11].

In this paper we aim to study the polarization structure behind the conoscopic images by performing a comprehensive analysis of the polarization state of the light transmitted through an NLC cell as a function of the incidence angles. Technically, we deal with a two-dimensional angular distribution of the Stokes parameters describing the field of polarization ellipses, which might be called the *polarization resolved conoscopic (angular) pattern*.

It was originally recognized by Nye [12–14] that the important elements characterizing the geometric structure of such polarization fields are the so-called *polarization singularities*. In particular, these are the *C-points* (the points where the light wave is circularly polarized) and the *L-lines* (the curves along which the polarization is linear). Over the past two decades these singularities and related issues have been the subject of numerous theoretical, experimental and numerical studies [15–27].

The theory of polarization singularities was applied to study the angular dependence of the polarization of plane wave eigenmodes in birefringent dichroic chiral crystals [28]. The polarization state of the electric displacement field was analysed in relation to the direction of the wavevector. This analysis was recently generalized and extended to a more complicated case of bianisotropic media [29].

The experimental results and theoretical analysis presented in [30] deal with the unfolding of a linearly polarized Laguerre–Gauss (LG_{01}) beam with an on-axis vortex on propagation through a birefringent crystal. It was found that a complicated pattern of polarization singularities is formed as a result of the anisotropy induced symmetry breaking.

In this study we adapt a systematic theoretical approach and explore the characteristic features of the polarization structure (the polarization resolved angular pattern) emerging from interference of four eigenmodes excited in NLC cells by plane waves with varying directions of incidence.

The layout of the paper is as follows. The problem of light transmission through a uniformly anisotropic NLC cell is exactly solved in section 2. Using the 4×4 matrix formalism and the orthogonality relations we deduce the expressions for the transmission and reflection matrices. In section 3 the analytical results are employed to perform analysis of the polarization resolved conoscopic patterns at linearly polarized incident light.

The case of homeotropic NLC cells is treated in section 3.2. We show that there is a family of the concentric circles each containing four symmetrically arranged C-points of alternating handedness. For these C-points, we obtain the formulae for the topological index and for the discriminant whose sign determines the type of the point according to the line classification. The index and the handedness of the C-points are found to alternate in sign along the radial direction. The morphology of the C-points lying on the circle of the smallest radius representing the direction close to the normal incidence is shown to be of the *lemon* type with the index equal to $+1/2$. In sufficiently thick cells, other C-points are either of the *star* type (the index is $-1/2$) or of the *monstar* type (the index is $+1/2$). The L-lines are formed by two rotated coordinate axes and by circles separating the circles with the C-points. Some numerical results for the tilted, planar and biaxial structures are presented in section 3.3. Discussion and concluding remarks are given in section 4.

2. Transmission of light through liquid crystal cells

We consider a nematic liquid crystal (NLC) cell of thickness d sandwiched between two parallel plates that are normal to the z axis: $z = 0$ and $z = d$. The NLC represents a birefringent material with the dielectric tensor given by

$$\boldsymbol{\varepsilon} = \epsilon_3 \mathcal{I}_3 + \Delta\epsilon_1 \hat{\mathbf{d}} \otimes \hat{\mathbf{d}} + \Delta\epsilon_2 \hat{\mathbf{m}} \otimes \hat{\mathbf{m}}, \tag{1}$$

where $\Delta\epsilon_i = \epsilon_i - \epsilon_3$ and $\mathcal{I}_n$ is the $n \times n$ identity matrix. In what follows carets will denote unit vectors.

Typically, anisotropy of nematics is locally uniaxial and NLC molecules align on average along a local unit director [1]. In this case the NLC director $\hat{\mathbf{d}}$ determines the optic axis and the expression (1) taken in the limit of vanishing biaxiality with $\Delta\epsilon_2 = 0$ gives the uniaxially anisotropic dielectric tensor. Its two principal values $\epsilon_3 \equiv \epsilon_\perp$ and $\epsilon_1 \equiv \epsilon_\parallel$ define the ordinary and extraordinary refractive indices, $n_o = \sqrt{\mu\epsilon_\perp}$ and $n_e = \sqrt{\mu\epsilon_\parallel}$, where μ is the NLC magnetic permeability.

In a more general case of biaxial nematics [31, 32] that were recently observed experimentally [6, 33], there are three different dielectric constants ϵ_1, ϵ_2 and ϵ_3 representing the eigenvalues of the dielectric tensor (1), so that the eigenvectors $\hat{\mathbf{d}}$, $\hat{\mathbf{m}}$ and $\hat{\mathbf{l}} = \hat{\mathbf{d}} \times \hat{\mathbf{m}}$ give the corresponding principal axes. The unit vectors $\hat{\mathbf{d}}$, $\hat{\mathbf{m}}$ and $\hat{\mathbf{l}}$ can be conveniently expressed in terms of Euler angles as follows:

$$\hat{\mathbf{d}} = \sin\theta_\mathrm{d}\cos\phi_\mathrm{d}\hat{\mathbf{x}} + \sin\theta_\mathrm{d}\sin\phi_\mathrm{d}\hat{\mathbf{y}} + \cos\theta_\mathrm{d}\hat{\mathbf{z}}, \tag{2a}$$

$$\hat{\mathbf{m}} = \cos\gamma_\mathrm{d}\mathbf{e}_x(\hat{\mathbf{d}}) + \sin\gamma_\mathrm{d}\mathbf{e}_y(\hat{\mathbf{d}}), \tag{2b}$$

$$\hat{\mathbf{l}} = -\sin\gamma_\mathrm{d}\mathbf{e}_x(\hat{\mathbf{d}}) + \cos\gamma_\mathrm{d}\mathbf{e}_y(\hat{\mathbf{d}}), \tag{2c}$$

where $\mathbf{e}_x(\hat{\mathbf{d}}) = (\cos\theta_\mathrm{d}\cos\phi_\mathrm{d}, \cos\theta_\mathrm{d}\sin\phi_\mathrm{d}, -\sin\theta_\mathrm{d})$ and $\mathbf{e}_y(\hat{\mathbf{d}}) = (-\sin\phi_\mathrm{d}, \cos\phi_\mathrm{d}, 0)$.

We shall need to write the Maxwell equations for a harmonic electromagnetic wave (the time-dependent factor is $\exp\{-\mathrm{i}\omega t\}$) in the form

$$\begin{aligned} \nabla \times \mathbf{E} &= \mathrm{i}\mu k_\mathrm{vac}\mathbf{H}, \\ \nabla \times \mathbf{H} &= -\mathrm{i}k_\mathrm{vac}\mathbf{D}, \end{aligned} \tag{3}$$

where $k_\mathrm{vac} = \omega/c$ is the free-space wavenumber; μ is the magnetic permittivity and $\mathbf{D} = \boldsymbol{\varepsilon} \cdot \mathbf{E}$ is the electric displacement field. The medium surrounding the NLC cell is assumed to be optically isotropic and characterized by the dielectric constant ϵ_m and the magnetic permittivity μ_m. So, the Maxwell equations in the region outside the cell are given by equations (3) with $\mu \to \mu_\mathrm{m}$ and $\mathbf{D} \to \epsilon_\mathrm{m}\mathbf{E}$.

Referring to figure 1, there are two plane waves in the lower half space $z \leqslant 0$ bounded by the entrance face of the NLC cell: the *incoming incident wave* $\{\mathbf{E}_\mathrm{inc}, \mathbf{H}_\mathrm{inc}\}$ and the *outgoing reflected wave* $\{\mathbf{E}_\mathrm{refl}, \mathbf{H}_\mathrm{refl}\}$. The *transmitted plane wave* $\{\mathbf{E}_\mathrm{tr}, \mathbf{H}_\mathrm{tr}\}$ is excited by the incident wave and propagates along the direction of incidence in the upper half space $z \geqslant d$ after the exit face. So, the electric field outside the cell is a superposition of the plane wave solutions of the Maxwell equations

$$\mathbf{E}|_{z<0} = \mathbf{E}_\mathrm{inc}(\hat{\mathbf{k}}_\mathrm{inc})\mathrm{e}^{\mathrm{i}(\mathbf{k}_\mathrm{inc}\cdot\mathbf{r})} + \mathbf{E}_\mathrm{refl}(\hat{\mathbf{k}}_\mathrm{refl})\mathrm{e}^{\mathrm{i}(\mathbf{k}_\mathrm{refl}\cdot\mathbf{r})}, \tag{4a}$$

$$\mathbf{E}|_{z>d} = \mathbf{E}_\mathrm{tr}(\hat{\mathbf{k}}_\mathrm{tr})\mathrm{e}^{\mathrm{i}(\mathbf{k}_\mathrm{tr}\cdot\mathbf{r})}. \tag{4b}$$

The wavevectors $\mathbf{k}_\mathrm{inc}$, $\mathbf{k}_\mathrm{refl}$ and $\mathbf{k}_\mathrm{tr}$ are constrained to lie in the plane of incidence due to the boundary conditions which require the tangential components of the electric and magnetic fields to be continuous at the boundary (interface) surfaces. These conditions are given by

$$\begin{aligned} \mathcal{P}(\hat{\mathbf{z}}) \cdot [\mathbf{E}|_{z=0+0} - \mathbf{E}|_{z=0-0}] &= \mathcal{P}(\hat{\mathbf{z}}) \cdot [\mathbf{E}|_{z=d+0} - \mathbf{E}|_{z=d-0}] = 0, \\ \mathcal{P}(\hat{\mathbf{z}}) \cdot [\mathbf{H}|_{z=0+0} - \mathbf{H}|_{z=0-0}] &= \mathcal{P}(\hat{\mathbf{z}}) \cdot [\mathbf{H}|_{z=d+0} - \mathbf{H}|_{z=d-0}] = 0, \end{aligned} \tag{5}$$

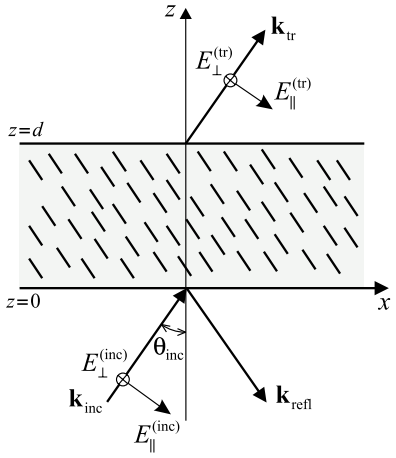

Figure 1. Geometry of nematic cell in the plane of incidence.

where $\mathcal{P}(\hat{\mathbf{z}}) = \mathcal{I}_3 - \hat{\mathbf{z}} \otimes \hat{\mathbf{z}}$ is the projector onto the plane with the normal directed along the vector $\hat{\mathbf{z}}$ (the x–y plane).

Another consequence of the boundary conditions (5) is that the tangential components of the wavevectors are the same. Assuming that the incidence plane is the x–z plane we have

$$\mathbf{k}_\alpha = k_{\rm m}\hat{\mathbf{k}}_\alpha = k_x\hat{\mathbf{x}} + k_z^{(\alpha)}\hat{\mathbf{z}}, \qquad \alpha \in \{\text{inc, refl, tr}\}, \tag{6}$$

$$k_x = k_{\rm m}\sin\theta_{\rm inc}, \qquad k_z^{(\rm inc)} = k_z^{(\rm tr)} = -k_z^{(\rm refl)} = k_{\rm m}\cos\theta_{\rm inc}, \tag{7}$$

where $k_{\rm m}/k_{\rm vac} = n_{\rm m} = \sqrt{\mu_{\rm m}\epsilon_{\rm m}}$ is the refractive index of the ambient medium and $\theta_{\rm inc}$ is the *incidence angle* (see figure 1).

The plane wave travelling in the isotropic ambient medium along the wavevector (6) is transverse, so that the polarization vectors of the electric and magnetic fields are given by

$$\begin{aligned} &\mathbf{E}_\alpha(\hat{\mathbf{k}}_\alpha) = E_\parallel^{(\alpha)}\mathbf{e}_x(\hat{\mathbf{k}}_\alpha) + E_\perp^{(\alpha)}\mathbf{e}_y(\hat{\mathbf{k}}_\alpha), \qquad \mathbf{e}_x(\hat{\mathbf{k}}_\alpha) = k_{\rm m}^{-1}(k_z^{(\alpha)}\hat{\mathbf{x}} - k_x\hat{\mathbf{z}}),\\ &\mu_{\rm m}\mathbf{H}_\alpha(\hat{\mathbf{k}}_\alpha) = \mathbf{q}_\alpha \times \mathbf{E}_\alpha(\hat{\mathbf{k}}_\alpha), \qquad \mathbf{q}_\alpha = k_{\rm vac}^{-1}\mathbf{k}_\alpha = n_{\rm m}\hat{\mathbf{k}}_\alpha \end{aligned} \tag{8}$$

where $\mathbf{q}_\alpha = k_{\rm vac}^{-1}\mathbf{k}_\alpha = n_{\rm m}\hat{\mathbf{k}}_\alpha$, $\mathbf{e}_y(\hat{\mathbf{k}}_\alpha) = \hat{\mathbf{y}}$ and $E_\parallel^{(\alpha)}$ ($E_\perp^{(\alpha)}$) is the in-plane (out-of-plane) component of the electric field.

2.1. Operator of evolution and transmission matrix

Owing to the conservation law for the tangential component of the wavevectors (6), the electromagnetic field of incident, transmitted and reflected waves (4*a*), (4*b*) propagating in the ambient medium is of the general form

$$\mathbf{E}(x, z) = \mathbf{E}(z)\mathrm{e}^{\mathrm{i}k_x x}, \qquad \mathbf{H}(x, z) = \mathbf{H}(z)\mathrm{e}^{\mathrm{i}k_x x}. \tag{9}$$

When the dielectric tensor (1) is independent of the in-plane coordinates, equation (9) remains applicable for the field inside the NLC cell.

The boundary conditions (5) can be conveniently written using the matrix notations as follows:

$$\mathbf{F}_< = \mathcal{Q}_{\rm m}\begin{pmatrix}\mathbf{E}_{\rm inc}\\ \mathbf{E}_{\rm refl}\end{pmatrix}\mathbf{F}(0), \qquad \mathbf{F}_> = \mathcal{Q}_{\rm m}\begin{pmatrix}\mathbf{E}_{\rm tr}\\ \mathbf{0}\end{pmatrix} = \mathbf{F}(d), \tag{10}$$

where

$$\mathbf{F}(z) \equiv \begin{pmatrix} E_x(z) \\ E_y(z) \\ H_y(z) \\ -H_x(z) \end{pmatrix}, \qquad \mathbf{E}_\alpha \equiv \begin{pmatrix} E_\parallel^{(\alpha)} \\ E_\perp^{(\alpha)} \end{pmatrix}, \tag{11}$$

that can be regarded as a version of the well known 4×4 matrix formalism [34, 35].

The matrix

$$\mathcal{Q}_\mathrm{m} = \begin{pmatrix} \mathcal{E}_+^{(m)} & \mathcal{E}_-^{(m)} \\ \mathcal{H}_+^{(m)} & \mathcal{H}_-^{(m)} \end{pmatrix} \tag{12}$$

relates the field vectors, $\mathbf{F}_< \equiv \mathbf{F}(0-0)$ and $\mathbf{F}_> \equiv \mathbf{F}(d+0)$, and the vector amplitudes $\mathbf{E}_\alpha$ of the waves in the surrounding medium. The block structure of $\mathcal{Q}_\mathrm{m}$ (12) is characterized by the four 2×2 matrices:

$$\begin{aligned} \mathcal{H}_+^{(m)} &= \boldsymbol{\sigma}_3 \mathcal{H}_-^{(m)} = \mu_\mathrm{m}^{-1} n_\mathrm{m} \mathcal{A}, & \mathcal{A} &= \mathrm{diag}(1, \cos\theta_\mathrm{inc}), \\ \mathcal{E}_+^{(m)} &= -\boldsymbol{\sigma}_3 \mathcal{E}_-^{(m)} = \mu_\mathrm{m}^{-1} n_\mathrm{m} \mathcal{B}, & \mathcal{B} &= \mu_\mathrm{m} n_\mathrm{m}^{-1}\, \mathrm{diag}(\cos\theta_\mathrm{inc}, 1), \end{aligned} \tag{13}$$

where $\boldsymbol{\sigma}_3 = \mathrm{diag}(1, -1)$.

It is rather straightforward to check the validity of the algebraic identities for the matrices (13)

$$[\mathcal{E}_\mu^{(\mathrm{m})}]^\dagger \mathcal{H}_\nu^{(\mathrm{m})} + [\mathcal{H}_\mu^{(\mathrm{m})}]^\dagger \mathcal{E}_\nu^{(\mathrm{m})} = \delta_{\mu\nu} \mathcal{N}_\mu^{(m)}, \qquad \mu, \nu \in \{+, -\}, \tag{14}$$

where $\mathcal{N}_\pm^{(m)} = \pm N_\mathrm{m} \mathcal{I}_2$, $N_\mathrm{m} = 2\mu_\mathrm{m}^{-1} n_\mathrm{m} \cos\theta_\mathrm{inc}$, $\delta_{\mu\nu}$ is the Kronecker symbol and the superscript † indicates Hermitian conjugation.

The identities (14) exemplify the *orthogonality relations* which are algebraic consequences of the conservation law for the energy flux in non-absorbing media [36]. In the case of one-dimensional inhomogeneity, this law requires the z component of the Poynting vector to be independent of z, leading to the orthogonality relations of the following 4×4 matrix form:

$$[\mathcal{Q}_\mathrm{m}]^\dagger \mathcal{G} \mathcal{Q}_\mathrm{m} = \mathcal{N}_\mathrm{m}, \qquad \mathcal{G} \equiv \begin{pmatrix} \mathbf{0} & \mathcal{I}_2 \\ \mathcal{I}_2 & \mathbf{0} \end{pmatrix}, \tag{15}$$

where $\mathcal{N}_\mathrm{m}$ is the diagonal matrix. Substituting $\mathcal{N}_\mathrm{m} = N_\mathrm{m}\, \mathrm{diag}(\mathcal{I}_2, -\mathcal{I}_2)$ into the orthogonality relations (15) recovers equation (14). Algebraically, equation (15) can be used to simplify inversion of the matrix $\mathcal{Q}_\mathrm{m}$ and to ease qualitative analysis (a more extended discussion of applications can be found, e.g., in [37]).

Given the characteristics of the incident wave and the boundary conditions (10), computing the amplitudes of the reflected and transmitted waves requires the electromagnetic field within the NLC cell to be found. At this stage we just note that, for the in-plane components of the electric and magnetic field, $\{E_x, E_y\}$ and $\{H_x, H_y\}$, the result can be presented in the form of a general solution to the linear problem

$$\mathbf{F}(z) = \mathcal{U}(z) \mathbf{F}(0), \tag{16}$$

where the matrix-valued function $\mathcal{U}(z)$ is the *evolution operator* which can be computed by solving the Maxwell equations (3).

We can now substitute (16) into the boundary conditions (10) and use the orthogonality relation (14) to deduce the relation linking the vector amplitudes of the three waves

$$\begin{pmatrix} \mathbf{E}_\mathrm{inc} \\ \mathbf{E}_\mathrm{refl} \end{pmatrix} = \mathcal{V} \begin{pmatrix} \mathbf{E}_\mathrm{tr} \\ \mathbf{0} \end{pmatrix}, \tag{17}$$

$$\mathcal{V} = \mathcal{N}_\mathrm{m}^{-1} [\mathcal{Q}_\mathrm{m}]^\dagger \mathcal{G} \mathcal{U}^{-1} \mathcal{Q}_\mathrm{m} = \begin{pmatrix} \mathcal{V}_{ee} & \mathcal{V}_{eh} \\ \mathcal{V}_{he} & \mathcal{V}_{hh} \end{pmatrix}, \tag{18}$$

where $\mathcal{U}^{-1} \equiv \mathcal{U}^{-1}(d)$.

From equation (17), we have

$$\begin{pmatrix} E_{\parallel}^{(\mathrm{tr})} \\ E_{\perp}^{(\mathrm{tr})} \end{pmatrix} = \mathcal{T} \begin{pmatrix} E_{\parallel}^{(\mathrm{inc})} \\ E_{\perp}^{(\mathrm{inc})} \end{pmatrix}, \qquad \mathcal{T} = \mathcal{V}_{ee}^{-1}, \tag{19}$$

where $\mathcal{T}$ is the *transmission (transfer) matrix* linking transmitted and incident waves.

A similar result for the reflected wave reads

$$\begin{pmatrix} E_{\parallel}^{(\mathrm{refl})} \\ E_{\perp}^{(\mathrm{refl})} \end{pmatrix} = \mathcal{R} \begin{pmatrix} E_{\parallel}^{(\mathrm{inc})} \\ E_{\perp}^{(\mathrm{inc})} \end{pmatrix}, \qquad \mathcal{R} = \mathcal{V}_{he}\mathcal{V}_{ee}^{-1} = \mathcal{V}_{he}\mathcal{T}, \tag{20}$$

where $\mathcal{R}$ is the *reflection matrix*.

So, we have both matrices expressed in terms of the evolution operator (16) describing spatial variations of the electromagnetic field within the optically anisotropic layer. It is instructive to see how this operator can be derived using the basis of *eigenmodes (normal modes)*. We concentrate on the case of a uniformly anisotropic medium, when the eigenmodes are known to be linearly polarized plane waves characterized by the $\hat{\mathbf{k}}$ dependent refractive indices [38–40].

2.2. Eigenmodes

Owing to the Maxwell equations (3), the electric displacement field of plane waves is transverse, $(\mathbf{D}\cdot\mathbf{k}) = 0$. So, assuming that the wavevector $\mathbf{k}$ lies in the plane of incidence (the x–z plane), the vector $\mathbf{D}$ can be conveniently defined by its components in the basis $\{e_x(\hat{\mathbf{k}}), e_y(\hat{\mathbf{k}}), e_z(\hat{\mathbf{k}}) \equiv \hat{\mathbf{k}} = k^{-1}(k_x\hat{\mathbf{x}} + k_z\hat{\mathbf{z}})\}$

$$\mathbf{D} = D_x e_x(\hat{\mathbf{k}}) + D_y e_y(\hat{\mathbf{k}}), \tag{21}$$

where $e_x(\hat{\mathbf{k}}) = k^{-1}(k_z\hat{\mathbf{x}} - k_x\hat{\mathbf{z}})$ and $e_y(\hat{\mathbf{k}}) = \hat{\mathbf{y}}$. For convenience, we shall often use the vector $\mathbf{q} = k_{\mathrm{vac}}^{-1}\mathbf{k}$, where length is equal to the refractive index, $q = n$, in place of the wavevector $\mathbf{k}$.

Given the electric displacement field (21), the electric field can be found from the constitutive relation

$$\mathbf{E} = \mu\boldsymbol{\eta}\cdot\mathbf{D}, \qquad \boldsymbol{\eta} = \eta_3\mathcal{I}_3 + \Delta\eta_1\hat{\mathbf{d}}\otimes\hat{\mathbf{d}} + \Delta\eta_2\hat{\mathbf{m}}\otimes\hat{\mathbf{m}}, \tag{22}$$

where $\eta_i = (\mu\epsilon_i)^{-1}$, $\Delta\eta_i = \eta_i - \eta_3$ and $\mu\boldsymbol{\eta}$ is the inverse dielectric tensor ($\mu\boldsymbol{\eta}\cdot\boldsymbol{\varepsilon} = \mathcal{I}_3$).

The Maxwell equations can now be combined with the relation (22) to yield the equation for the displacement vector $\mathbf{D}$ in the form of an eigenvalue problem

$$\boldsymbol{\eta}_t\cdot\mathbf{D} = q^{-2}\mathbf{D}, \qquad \boldsymbol{\eta}_t = \mathcal{P}(\hat{\mathbf{k}})\cdot\boldsymbol{\eta}\cdot\mathcal{P}(\hat{\mathbf{k}}), \tag{23}$$

where $\mathcal{P}(\hat{\mathbf{k}}) = \mathcal{I}_3 - \hat{\mathbf{k}}\otimes\hat{\mathbf{k}}$ is the projector onto the plane normal to the wavevector $\mathbf{k}$. By using the expression for the inverse dielectric tensor (22) we can rewrite equation (23) in the explicit matrix form:

$$[a_-\boldsymbol{\sigma}_3 + b\boldsymbol{\sigma}_1 - \lambda\mathcal{I}_2]\begin{pmatrix} D_x \\ D_y \end{pmatrix} = \mathbf{0}, \qquad \boldsymbol{\sigma}_1 = \begin{pmatrix} 0 & 1 \\ 1 & 0 \end{pmatrix}, \tag{24}$$

$$2a_{\mp} = \Delta\eta_1(\tilde{d}_x^2 \mp \tilde{d}_y^2) + \Delta\eta_2(\tilde{m}_x^2 \mp \tilde{m}_y^2), \tag{25}$$

$$b = \Delta\eta_1\tilde{d}_x\tilde{d}_y + \Delta\eta_2\tilde{m}_x\tilde{m}_y, \qquad \lambda = 1 - \eta_3 q^2 - a_+, \tag{26}$$

where $\tilde{d}_{x,y} = q(\hat{\mathbf{d}}\cdot e_{x,y}(\hat{\mathbf{k}}))$ and $\tilde{m}_{x,y} = q(\hat{\mathbf{m}}\cdot e_{x,y}(\hat{\mathbf{k}}))$. Then the dispersion relation (Fresnel's equation)

$$(1-\eta_3 q^2)[1 - \eta_3 q^2 - \Delta\eta_1(q^2 - \tilde{d}_z^2) - \Delta\eta_2(q^2 - \tilde{m}_z^2)] + \Delta\eta_1\Delta\eta_2 q^2\tilde{l}_z^2 = 0, \tag{27}$$

where $q\tilde{l}_z = \tilde{d}_x\tilde{m}_y - \tilde{d}_y\tilde{m}_x = q^2(\hat{\mathbf{l}}\cdot\hat{\mathbf{k}})$, can be derived as the condition for the system of linear equations (24) to have a non-vanishing solution.

The Fresnel equation describes the wave surface. In our case solving the algebraic equation (27) at $q_x = n_{\rm m} \sin\theta_{\rm inc}$ gives the values of the z component of the vector $\mathbf{q}$, q_z.

Generally, there are four roots of equation (27) $q_z^{(\alpha)}$. Each root corresponds to the eigenwave propagating inside the cell with the wavevector $\mathbf{k}_\alpha = k_{\rm vac}(q_x, 0, q_z^{(\alpha)})$ and the refractive index $n_\alpha = q_\alpha$. The corresponding polarization vector of the electric displacement field is given by

$$\mathbf{D}^{(\alpha)} = \begin{cases} \cos\phi_\alpha e_x(\hat{\mathbf{k}}_\alpha) + \sin\phi_\alpha e_y(\hat{\mathbf{k}}_\alpha), & \lambda_\alpha > 0 \\ -\sin\phi_\alpha e_x(\hat{\mathbf{k}}_\alpha) + \cos\phi_\alpha e_y(\hat{\mathbf{k}}_\alpha), & \lambda_\alpha < 0, \end{cases} \tag{28}$$

where $\lambda_\alpha = \lambda|_{q_z=q_z^{(\alpha)}}$ and $2\phi_\alpha = \arg(a_- + {\rm i}b)|_{q_z=q_z^{(\alpha)}}$.

Note that the azimuthal angle ϕ_α becomes indeterminate in the degenerate case when the coefficients a_- and b are both identically equal to zero. Typically, as far as the eigenmodes are concerned, this case does not present any fundamental difficulties. It just means that the azimuthal angles of the degenerate eigenmodes can be prescribed arbitrarily. Such freedom of choice, however, does not affect the evolution operator, which remains uniquely defined.

The procedure to determine the characteristics of the eigenmodes involves the following steps: (a) evaluation of q_z by solving the Fresnel equation (27); (b) calculation of the polarization vectors of the electric displacement field $\mathbf{D}^{(\alpha)}$ by using the formula (28); (c) computing the polarization vectors of the electric and magnetic fields from the relations: $\mathbf{E}^{(\alpha)} = \mu\boldsymbol{\eta}\cdot\mathbf{D}^{(\alpha)}$ (see equation (22)) and $\mu\mathbf{H}^{(\alpha)} = \mathbf{q}_\alpha \times \mathbf{E}^{(\alpha)}$ (see equation (8)).

2.2.1. Uniaxial anisotropy. Now we apply the above procedure to the limiting case of uniaxial anisotropy with $\epsilon_2 = \epsilon_3$ and $\Delta\epsilon_2 = \Delta\eta_2 = 0$. At $\Delta\eta_2 = 0$, the Fresnel equation (27) takes the factorized form and the values of q_z can be found as roots of two quadratic equations.

The first equation $1 - \eta_3 q^2 = 0$ represents the spherical wave surface. The corresponding eigenmodes are known as the *ordinary waves*. There are two values of q_z,

$$q_z^{(\pm o)} = \pm\sqrt{n_\perp^2 - q_x^2}, \tag{29}$$

where $n_\perp^2 = \mu\epsilon_3 \equiv \mu\epsilon_\perp$, that are equal in value but opposite in sign. When, similar to the incident and transmitted waves, the z component of the wavevector (and the vector $\mathbf{q}$) is positive, the eigenmode might be called the *refracted (forward) eigenwave*. In the opposite case, where, similar to the reflected wave, $q_z^{(\alpha)}$ is negative, the eigenmode will be referred to as the *reflected (backward) eigenwave*. So, equation (29) describes two ordinary eigenmodes: the refracted eigenwave with $q_z = q_z^{(+o)} > 0$ and the reflected eigenwave with $q_z = q_z^{(-o)} < 0$.

The second equation

$$q^2 + u_a(\mathbf{q}\cdot\hat{\mathbf{d}})^2 - n_\parallel^2 = 0, \tag{30}$$

where $n_\parallel^2 = \mu\epsilon_1 \equiv \mu\epsilon_\parallel$ and $u_a = -\Delta\eta_1/\eta_1 = (n_\parallel^2 - n_\perp^2)/n_\perp^2$ is the *anisotropy parameter*, gives the values of q_z for the eigenmodes known as the *extraordinary waves*. These are given by

$$q_z^{(\pm e)} = [1 + u_a d_z^2]^{-1}\{-u_a d_z d_x q_x \pm \sqrt{D}\}, \tag{31}$$

where $D = n_\parallel^2(1 + u_a d_z^2) - q_x^2[1 + u_a(d_x^2 + d_z^2)]$, $d_x = (\hat{\mathbf{d}}\cdot\hat{\mathbf{x}})$ and $d_z = (\hat{\mathbf{d}}\cdot\hat{\mathbf{z}})$.

At $u_a > 0$ ($u_a < 0$), in the x–z plane, equation (30) describes the ellipse with the major (minor) semi-axis of length $n_\parallel$ oriented perpendicular to the projection of the director (2*a*) on the plane of incidence $(d_x, 0, d_z)$. The length of the minor (major) semi-axis, $\tilde{n}_\perp = [n_\perp^{-2} - u_a(d_y/n_\parallel)^2]^{-1/2}$, depends on the y component of the director and varies from $n_\perp$ to $n_\parallel$ as d_y^2 increases from zero to unity. Clearly, degeneracy in refractive indices with $n_o = n_{\pm e}$

may occur only if the director is in the incidence plane ($\phi_{\rm d} = 0$). Additionally, the matching condition for the x components of $\mathbf{q}$ and the director $q_x \equiv n_m \sin\theta_{\rm inc} = \pm n_o d_x \equiv \pm n_o \sin\theta_{\rm d}$ needs to be met.

The wavevectors and the refractive indices of the normal modes are determined by the relation

$$\mathbf{q}_{\pm\alpha} = k_{\rm vac}^{-1}\mathbf{k}_{\pm\alpha} = q_x\hat{\mathbf{x}} + q_z^{(\pm\alpha)}\hat{\mathbf{z}} = n_{\pm\alpha}\hat{\mathbf{k}}_{\pm\alpha}, \qquad \alpha \in \{o, e\}, \tag{32}$$

where $n_{\pm\alpha} = q_{\pm\alpha}$, $n_{\pm o} = n_o = n_\perp$ is the ordinary refractive index and $n_{\pm e}$ is the refractive index of the extraordinary wave propagating along the unit vector $\hat{\mathbf{k}}_{\pm e}$.

Substituting $\Delta\eta_2 = 0$ into equations (25)–(26) provides the relations

$$\operatorname{sign}\lambda_{\pm e} = -\operatorname{sign}\lambda_{\pm o} = \operatorname{sign}\Delta\eta_1, \qquad a_- + \mathrm{i}b = \Delta\eta_1(\tilde{d}_x + \mathrm{i}\tilde{d}_y)^2. \tag{33}$$

These can be combined with equation (28) to yield the well known result for the polarization vectors of the electric displacement field:

$$\mathbf{D}^{(\pm o)} \propto \hat{\mathbf{k}}_{\pm o} \times \hat{\mathbf{d}}, \qquad \mathbf{D}^{(\pm e)} \propto \mathcal{P}(\hat{\mathbf{k}}_{\pm e}) \cdot \hat{\mathbf{d}}. \tag{34}$$

Then, following the procedure described at the end of section 2.2, we find the polarization vectors of the electric field for the eigenmodes

$$\mathbf{E}^{(\pm o)} = -\mathbf{q}_{\pm o} \times \hat{\mathbf{d}}, \qquad \mathbf{E}^{(\pm e)} = [\hat{\mathbf{d}} - n_o^{-2}(\hat{\mathbf{d}} \cdot \mathbf{q}_{\pm e})\mathbf{q}_{\pm e}]. \tag{35}$$

The result for the magnetic field of the normal modes is

$$\mathbf{H}^{(\pm o)} = \mu^{-1}[n_o^2\hat{\mathbf{d}} - (\hat{\mathbf{d}} \cdot \mathbf{q}_{\pm o})\mathbf{q}_{\pm o}], \qquad \mathbf{H}^{(\pm e)} = \mu^{-1}\mathbf{q}_{\pm e} \times \hat{\mathbf{d}}. \tag{36}$$

By analogy with equation (12), we define the matrix composed of the polarization vectors as follows:

$$\mathcal{Q} = \begin{pmatrix} \mathcal{E}_+ & \mathcal{E}_- \\ \mathcal{H}_+ & \mathcal{H}_- \end{pmatrix}, \tag{37}$$

where

$$\mathcal{E}_\pm = \begin{pmatrix} E_x^{(\pm o)} & E_x^{(\pm e)} \\ E_y^{(\pm o)} & E_y^{(\pm e)} \end{pmatrix}, \qquad \mathcal{H}_\pm = \begin{pmatrix} H_y^{(\pm o)} & H_y^{(\pm e)} \\ -H_x^{(\pm o)} & -H_x^{(\pm e)} \end{pmatrix}. \tag{38}$$

The matrix of eigenvectors (37) along with the eigenvalues (29) and (31) can now be used to describe the z dependence of the in-plane components of the electromagnetic field inside the cell in terms of the eigenmode amplitudes. The result is given by

$$\mathbf{F}(z) = \mathcal{Q}\mathcal{U}_d(z)\begin{pmatrix} \boldsymbol{\beta}_+ \\ \boldsymbol{\beta}_- \end{pmatrix}, \qquad \mathcal{U}_d(z) = \begin{pmatrix} \mathcal{U}_d^{(+)}(z) & \mathbf{0} \\ \mathbf{0} & \mathcal{U}_d^{(-)}(z) \end{pmatrix}, \tag{39}$$

$$\mathcal{U}_d^{(\pm)}(z) = \operatorname{diag}(\exp[\mathrm{i}k_z^{(\pm o)}z], \exp[\mathrm{i}k_z^{(\pm e)}z]), \tag{40}$$

where $\boldsymbol{\beta}_\pm \equiv \binom{\beta_{\pm o}}{\beta_{\pm e}}$ are the columns representing the amplitudes of the eigenmodes.

2.2.2. Transmission and reflection matrices. Now it is not difficult to derive the evolution operator (16) from equation (39). We can also use the orthogonality relation (15) for the matrix (37) so as to obtain the following result:

$$\mathcal{U}(z) = \mathcal{Q}\mathcal{U}_d(z)\mathcal{Q}^{-1} = \mathcal{Q}\mathcal{U}_d(z)\mathcal{N}^{-1}\mathcal{Q}^\dagger\mathcal{G}, \tag{41}$$

where the matrix $\mathcal{G}$ is defined in equation (15), the matrix $\mathcal{N} = \mathcal{Q}^\dagger\mathcal{G}\mathcal{Q} = \operatorname{diag}(\mathcal{N}_+, \mathcal{N}_-)$ is diagonal and its non-vanishing elements

$$\mathcal{N}_\pm = \begin{pmatrix} N_{\pm o} & 0 \\ 0 & N_{\pm e} \end{pmatrix}, \qquad N_\alpha = 2(\hat{\mathbf{z}} \cdot \mathbf{E}^{(\alpha)} \times \mathbf{H}^{(\alpha)}) \tag{42}$$

are proportional to the normal components of the Poynting vector of the eigenmodes.

Note that the evolution operator is non-unitary. This is evident from the identity

$$\mathcal{U}^{-1}(z) = \mathcal{U}^{*}(z) = \mathcal{G}\mathcal{U}^{\dagger}(z)\mathcal{G}, \tag{43}$$

where an asterisk indicates complex conjugation, that immediately follows from expression (41).

The operator (41) can be substituted into the expression for the matrix $\mathcal{V}$ (18) to yield the transmission and reflection matrices given by equations (19) and (20), respectively. By using the identity (43), we deduce the relation for the matrix $\mathcal{V}$

$$\mathcal{V}^{-1} = \mathcal{V}^{*} = \mathcal{G}_3\mathcal{V}^{\dagger}\mathcal{G}_3, \qquad \mathcal{G}_3 = \mathrm{diag}(\mathcal{I}_2, -\mathcal{I}_2). \tag{44}$$

One of the most important consequences of equation (44) is the conservation law $\mathcal{T}^{\dagger}\mathcal{T} + \mathcal{R}^{\dagger}\mathcal{R} = \mathcal{I}_2$. In addition, it is clear that the transmission matrix (19) is symmetric.

The explicit formulas for the transmission and reflection matrices given by equations (19) and (20) can be obtained by substituting (41) into (18). After some straightforward algebraic manipulations we have

$$\mathcal{T} = 2\mu_{\mathrm{m}}n_{\mathrm{m}}^{-1}\cos\theta_{\mathrm{inc}}\boldsymbol{\tau}^{-1}, \qquad \boldsymbol{\tau} = \boldsymbol{\tau}_{+} + \boldsymbol{\tau}_{-}, \tag{45}$$

$$\mathcal{R} = \boldsymbol{\sigma}_3[\mathcal{B}_{+}\tilde{\mathcal{U}}_{+}[\mathcal{A}_{+}]^{\dagger} + \mathcal{B}_{-}\tilde{\mathcal{U}}_{-}[\mathcal{A}_{-}]^{\dagger}]\boldsymbol{\tau}^{-1}, \tag{46}$$

where

$$\boldsymbol{\tau}_{\pm} = \mathcal{A}_{\pm}\tilde{\mathcal{U}}_{\pm}[\mathcal{A}_{\pm}]^{\dagger}, \qquad \tilde{\mathcal{U}}_{\pm} = [\mathcal{U}_d^{(\pm)}(d)]^{*}\mathcal{N}_{\pm}^{-1}, \tag{47}$$

$$\mathcal{A}_{\pm} = \mathcal{B}\mathcal{H}_{\pm} + \mathcal{A}\mathcal{E}_{\pm}, \qquad \mathcal{B}_{\pm} = \mathcal{B}\mathcal{H}_{\pm} - \mathcal{A}\mathcal{E}_{\pm}. \tag{48}$$

The expressions for the electric and magnetic fields of the eigenmodes can be substituted into equation (42) to yield the diagonal elements of the matrices $\mathcal{N}_{+}$ and $\mathcal{N}_{-}$

$$\mu N_{\pm o} = 2q_z^{(\pm o)}[n_o^2 - (\mathbf{q}_{\pm o}\cdot\hat{\mathbf{d}})^2], \tag{49}$$

$$\mu N_{\pm e} = 2n_o^{-2}[d_z(\mathbf{q}_{\pm e}\cdot\hat{\mathbf{d}})(n_{\pm e}^2 - n_o^2) + q_z^{(\pm e)}(n_o^2 - (\mathbf{q}_{\pm e}\cdot\hat{\mathbf{d}})^2)]. \tag{50}$$

Equations (45)–(50), along with the matrices (38), $\mathcal{E}_{\pm}$ and $\mathcal{H}_{\pm}$, define the exact solution of the transmission/reflection problem in the 2×2 matrix form.

Note that diagonal (non-diagonal) elements of the matrices (38) are zero provided the director is normal (parallel) to the plane of incidence. In these cases, where either $d_y = 1$ or $d_y = 0$, the matrix $\boldsymbol{\tau}$ and the transmission matrix are both diagonal

$$\boldsymbol{\tau} = \mathrm{diag}(\tau_x, \tau_y), \qquad \mathcal{T} = \mathrm{diag}(t_x, t_y), \tag{51}$$

where $t_{x,y} = 2\mu_{\mathrm{m}}n_{\mathrm{m}}^{-1}\cos\theta_{\mathrm{inc}}\tau_{x,y}^{-1}$.

The simplest case occurs when the cell is homeotropically aligned and $d_z = 1$. For the homeotropic director structure, the elements of the matrix $\boldsymbol{\tau}$ are given by

$$\tau_x = 2\mu_{\mathrm{m}}n_{\mathrm{m}}^{-1}\cos\theta_{\mathrm{inc}}\cos\delta_e - \mathrm{i}[q_z^{(e)}]^{-1}\sin\delta_e[(\mu_{\mathrm{m}}n_o n_{\mathrm{m}}^{-1}\cos\theta_{\mathrm{inc}})^2 + (n_o^{-1}q_z^{(e)})^2], \tag{52a}$$

$$\tau_y = 2\mu_{\mathrm{m}}n_{\mathrm{m}}^{-1}\cos\theta_{\mathrm{inc}}\cos\delta_o - \mathrm{i}[q_z^{(o)}]^{-1}\sin\delta_o[\cos^2\theta_{\mathrm{inc}} + (\mu_{\mathrm{m}}n_{\mathrm{m}}^{-1}q_z^{(o)})^2], \tag{52b}$$

where $q_z^{(o)} = \sqrt{n_o^2 - q_x^2}$, $q_z^{(e)} = n_o n_{\parallel}^{-1}\sqrt{n_{\parallel}^2 - q_x^2}$ and $\delta_\alpha = q_z^{(\alpha)}k_{\mathrm{vac}}d$.

3. Angular structure of polarization ellipse field

Now we pass on to discussing how the polarization properties of the transmitted light depend on the direction of the incident wave. This direction is specified by two angles: the incidence angle θ_{inc} and the azimuthal angle of the plane of incidence ϕ_{inc}. Clearly, we need to replace the director azimuthal angle ϕ_{d} with $\phi_{\mathrm{d}} - \phi_{\mathrm{inc}}$ so as to have the Euler angles describing the orientation of the director (2) with respect to the incidence plane. The transmission matrix

$\mathcal{T}(\theta_{\rm inc}, \theta_{\rm d}, \phi_{\rm d})$ obtained in the previous section is thus changed to $\mathcal{T}(\theta_{\rm inc}, \theta_{\rm d}, \phi_{\rm d} - \phi_{\rm inc})$. In this section the dependence of the polarization parameters of transmitted waves on the angles $\theta_{\rm inc}$ and $\phi_{\rm inc}$ will be our primary concern.

We begin by introducing necessary parameters and notations. Much of this material can be found in standard textbooks such as [38, 40] (a more recent and extended discussion can be found, e.g., in [27]). The polarization state of a plane wave can be conveniently characterized by using the components of its vector amplitude in the spherical basis as follows:

$$\mathbf{E}(\hat{\mathbf{k}}) = E_+ \mathbf{e}_+(\hat{\mathbf{k}}) + E_- \mathbf{e}_-(\hat{\mathbf{k}}) = \mathrm{e}^{\mathrm{i}\phi_0}\{\mathbf{p}_+ + \mathrm{i}\mathbf{p}_-\}, \tag{53a}$$

$$E_\pm = 2^{-1/2}(E_\parallel \mp \mathrm{i}E_\perp) = |E_\pm| \exp\{\mathrm{i}\phi_\pm\}, \tag{53b}$$

$$\mathbf{p}_\pm = 2^{-1/2}\{|E_+| \pm |E_-|\}\mathbf{e}'_{x,y}(\hat{\mathbf{k}}), \qquad \phi_0 = (\phi_- + \phi_+)/2, \tag{53c}$$

where $\sqrt{2}\mathbf{e}_\pm(\hat{\mathbf{k}}) = \mathbf{e}_x(\hat{\mathbf{k}}) \pm \mathrm{i}\mathbf{e}_y(\hat{\mathbf{k}})$; the angle ϕ_0 is variously known as the *phase of the vibration* [12] or the *rectifying phase* [27]; $\mathbf{p}_+$ and $\mathbf{p}_-$ are the major and minor semiaxes of the polarization ellipse with the principal axes directed along the unit vectors $\mathbf{e}'_x(\hat{\mathbf{k}}) = \cos\phi_p \mathbf{e}_x(\hat{\mathbf{k}}) + \sin\phi_p \mathbf{e}_y(\hat{\mathbf{k}})$ and $\mathbf{e}'_y(\hat{\mathbf{k}}) = -\sin\phi_p \mathbf{e}_x(\hat{\mathbf{k}}) + \cos\phi_p \mathbf{e}_y(\hat{\mathbf{k}})$, respectively.

So, the angle

$$\phi_p = (\phi_- - \phi_+)/2 = 2^{-1}\arg([E_+]^* E_-) = 2^{-1}\arg(E_-/E_+) \tag{54}$$

specifies the orientation of the polarization ellipse and will be referred to as the *azimuthal angle of polarization* or the *polarization azimuth*. Another important characteristic of the polarization ellipse describing its eccentricity is the signed ellipticity parameter

$$\epsilon_{\rm ell} = \frac{|E_-| - |E_+|}{|E_-| + |E_+|}. \tag{55}$$

This parameter will be referred to as the *ellipticity* and its sign defines the handedness of the ellipse.

According to [38], the ellipse is considered to be right handed (RH) if its helicity is negative, $(\mathbf{p}_+ \times \mathbf{p}_- \cdot \hat{\mathbf{k}}) < 0$, so that $|E_+| < |E_-|$ and $\epsilon_{\rm ell} > 0$. For the left-handed (LH) ellipse, $(\mathbf{p}_+ \times \mathbf{p}_- \cdot \hat{\mathbf{k}}) > 0$ and $\epsilon_{\rm ell} < 0$.

Experimentally, the characteristics of the polarization ellipse can be obtained by measuring the Stokes parameters related to the *coherence matrix* with the elements $\mathcal{M}_{\alpha\beta} = E_\alpha {E_\beta}^*$, where $\alpha, \beta \in \{\parallel, \perp\}$. In a circular basis, this matrix can be written as a linear combination of the Pauli matrices. The coefficients of the combination are the Stokes parameters

$$\mathcal{M}_c = \mathcal{C}\mathcal{M}\mathcal{C}^\dagger = \begin{pmatrix} |E_+|^2 & E_+E_-^* \\ E_-E_+^* & |E_-|^2 \end{pmatrix} = 2^{-1}\sum_{i=0}^{4} S_i \boldsymbol{\sigma}_i, \tag{56}$$

where $\mathcal{C} = 2^{-1/2}\left(\begin{smallmatrix} 1 & -\mathrm{i} \\ 1 & i \end{smallmatrix}\right)$, $\boldsymbol{\sigma}_0 \equiv \mathcal{I}_2$ and $\boldsymbol{\sigma}_2 = \left(\begin{smallmatrix} 0 & -\mathrm{i} \\ \mathrm{i} & 0 \end{smallmatrix}\right)$. Since the determinant of the coherence matrix vanishes, $\det \mathcal{M} = 0$, the Stokes parameters lie on the four-dimensional cone $S_0^2 = \sum_{i=1}^3 S_i^2$, and can be parameterized as follows:

$$S_0 = |E_+|^2 + |E_-|^2 = |E_\parallel|^2 + |E_\perp|^2, \tag{57a}$$

$$S_1 = 2\,\mathrm{Re}\, E_+^* E_- = |E_\parallel|^2 - |E_\perp|^2 = S_0 \cos 2\chi_p \cos 2\phi_p, \tag{57b}$$

$$S_2 = 2\,\mathrm{Im}\, E_+^* E_- = 2\,\mathrm{Re}\, E_\perp E_\parallel^* = S_0 \cos 2\chi_p \sin 2\phi_p, \tag{57c}$$

$$S_3 = |E_+|^2 - |E_-|^2 = 2\,\mathrm{Im}\, E_\perp E_\parallel^* = S_0 \sin 2\chi_p, \tag{57d}$$

where $0 < \phi_p \leqslant \pi$ is the polarization azimuth (54) and $-\pi/4 \leqslant \chi_p \leqslant \pi/4$ is the ellipticity angle. Then, the relations expressing the ellipse characteristics in terms of the Stokes parameters are

$$\phi_p = 2^{-1}\arg S, \quad S \equiv S_1 + \mathrm{i}S_2, \tag{58}$$

$$\epsilon_{\rm ell} = -\tan\chi_p, \quad \chi_p = 2^{-1}\arcsin(S_3/S_0). \tag{59}$$

The important special case occurs when the wave is circularly polarized and $|E_\nu| = 0$, so that the phases ϕ_ν and ϕ_p are indeterminate. This is an example of the *polarization singularity* that, according to equation (58), can be regarded as the *phase singularity* of the complex Stokes field, $S = S_1 + \mathrm{i}S_2$. The point where the polarization is circular with $|E_\nu| = 0$ (and $\epsilon_{\mathrm{ell}} = \nu$) will be referred to as the C_ν *point*. In our case such points are characterized by the incidence angles at which the transmitted wave is circular polarized and $E_\nu^{(\mathrm{tr})} = 0$.

The case of the linearly polarized wave with $|E_+| = |E_-|$ provides another example of the polarization singularity where the handedness is undefined. The curves along which the polarization is linear are called the *L-lines*.

3.1. Angular patterns: C-points and L-lines

The transmission matrix in the circular basis

$$\mathcal{T}_c = \begin{pmatrix} t_{++} & t_{+-} \\ t_{-+} & t_{--} \end{pmatrix} = \mathcal{C}\mathcal{T}\mathcal{C}^\dagger \tag{60}$$

relates the circular components of the incident and transmitted waves, $\{E_+^{(\mathrm{inc})}, E_-^{(\mathrm{inc})}\}$ and $\{E_+^{(\mathrm{tr})}, E_-^{(\mathrm{tr})}\}$. Since the transmission matrix (45) is symmetric, the diagonal elements of the matrix (60) are equal, $t_{++} = t_{--} = (t_{xx} + t_{yy})/2$, whereas the non-diagonal elements are $t_{\pm\mp} = (t_{xx} - t_{yy})/2 \mp t_{xy}$. The transmission matrix

$$\tilde{\mathcal{T}}(\rho, \phi) = \exp(-\mathrm{i}\phi\boldsymbol{\sigma}_3)\mathcal{T}_c(\rho, \phi)\exp(\mathrm{i}\phi\boldsymbol{\sigma}_3), \tag{61}$$

$$\rho = r\tan\theta_{\mathrm{inc}}, \qquad \phi = \phi_{\mathrm{inc}} \tag{62}$$

describes the conoscopic patterns on the transverse plane of projection (*the plane of observation*), where ρ and ϕ are the polar coordinates ($x = \rho\cos\phi$ and $y = \rho\sin\phi$ are the Cartesian coordinates) and r is the factor determining the length scale in the observation plane that depends on the characteristics of the projecting system such as focal lengths and the aperture.

We concentrate on the case in which the incident plane wave is linearly polarized along the unit vector: $\cos\psi_p\mathbf{e}_x(\hat{\mathbf{k}}_{\mathrm{inc}}) + \sin\psi_p\mathbf{e}_y(\hat{\mathbf{k}}_{\mathrm{inc}})$. For the incident wave with the circular components $E_\nu^{(\mathrm{inc})} = \exp(-\nu\psi_p)|E_{\mathrm{inc}}|$, the reduced components of the transmitted wave are given by

$$E_\nu^{(\mathrm{tr})}/|E_{\mathrm{inc}}| \equiv \Psi_\nu/2 = [t_{\nu,\nu} + t_{\nu,-\nu}\exp(-2\mathrm{i}\nu\psi)]\exp(-\mathrm{i}\nu\psi_p), \tag{63}$$

where $\psi = \phi - \psi_p$.

The polar coordinates of the C_ν points on the observation plane, $\rho_k^{(\nu)}$ and $\phi_k^{(\nu)}$, where k is the numbering label, can be found by solving the equation

$$|\Psi_\nu(\rho, \phi)| = 0 \tag{64}$$

that generally has multiple solutions.

The C_ν points can be viewed as the phase singularities of the complex scalar field

$$\tilde{S} = \Psi_+^*\Psi_- = \tilde{S}_1 + \mathrm{i}\tilde{S}_2 \tag{65}$$

proportional to the Stokes field defined in equation (58). Such singularities are characterized by the *winding number*, which is the signed number of rotations of the two-component field $(\tilde{S}_1, \tilde{S}_2)$ around the circuit surrounding the singularity [41]. The winding number, also known as the *signed strength of the dislocation*, is generically ± 1.

Since the polarization azimuth (58) is defined modulo π and $2\phi_p = \arg\tilde{S}$, the dislocation strength is twice the index of the corresponding C_ν point, I_C. For generic C-points, $I_C = \pm 1/2$ and the index can be computed from the formula

$$I_C = \tfrac{1}{2}\,\mathrm{sign}[\mathrm{Im}(\partial_x\tilde{S}^*\partial_y\tilde{S})]_{x=x_\nu, y=y_\nu}, \tag{66}$$

where $\partial_x f$ is the partial derivative of f with respect to x.

The relation (66) gives the index of the C_ν point with the coordinates (x_ν, y_ν) expressed in terms of the vorticity [20, 27]: $\mathrm{Im}(\partial_x \tilde{S}^* \partial_y \tilde{S}) = \partial_x \tilde{S}_1 \partial_y \tilde{S}_2 - \partial_y \tilde{S}_1 \partial_x \tilde{S}_2$. The formula linking gradients of the complex field $(\mathbf{E} \cdot \mathbf{E}) \propto \Psi_+ \Psi_-$ and the index for C-lines in the three-dimensional space was derived in [42].

If $\Psi_\nu = 0$ (C_ν-point), only derivatives of Ψ_ν enter expression (66), which can be suitably rearranged to yield the index of the C_ν-point in the following form:

$$I_C = \frac{\nu}{2}\mathrm{sign}[\mathrm{Im}(\partial_x \Psi_\nu \partial_y \Psi_\nu^*)]_{x=x_\nu, y=y_\nu} = \frac{\nu}{2}\mathrm{sign}[\mathrm{Im}(\partial_\rho \Psi_\nu \partial_\phi \Psi_\nu^*)]_{\rho=\rho_\nu, \phi=\phi_\nu}. \tag{67}$$

Subsequently, we shall apply the formula (67) expressing the index in terms of the derivatives with respect to polar coordinates to the case of the homeotropically aligned cell.

In addition to the handedness and the index, the C-points are classified according to the number of straight lines terminating on the singularity. This is the so-called *line classification* that was initially studied in the context of umbilic points [43].

For generic C-points, the number of straight lines, N_C, may either be one or three. This number is three provided the index equals $-1/2$, $I_C = -1/2$, and such C-points are called *stars* (see figure 2(a)). When the index is $+1/2$, there are two characteristic patterns of polarization ellipses around the C-points. These are depicted in figures 2(b) and (c) and correspond to the C-points known as the *lemons* ($N_C = 1$) and the *monstars* ($N_C = 3$), respectively [12]. The quantitative criterion to distinguish between the C-points of the lemon and the monstar types was deduced in [27].

We conclude this subsection with the remark that the transmitted wave is linearly polarized when the condition

$$|\Psi_+(\rho, \phi)| = |\Psi_-(\rho, \phi)| \tag{68}$$

is satisfied. So, equation (68) describes loci of points forming the L-lines lying in the projection plane.

3.2. Homeotropic cell

When the director is normal to the substrates, the NLC cell is homeotropically aligned and $d_z = 1$. In this case the transmission matrix is diagonal and the circular components of the transmitted light are given by

$$\Psi_\nu = [(t_x + t_y) + (t_x - t_y)\exp(-2\mathrm{i}\nu\psi)]\exp(-\mathrm{i}\nu\psi_p), \tag{69}$$

where the transmission coefficients $t_{x,y} = t_{x,y}(\theta_{\mathrm{inc}}) \equiv t_{x,y}(\rho)$ do not depend on the azimuthal angle of the incidence plane $\phi \equiv \phi_{\mathrm{inc}}$ and are defined in equations (51), (52*a*) and (52*b*).

From (69), the C-points may appear at the incidence angles θ_{inc} that satisfy the condition $|t_x + t_y| = |t_x - t_y|$. Another form of this condition

$$R(\rho) \equiv \mathrm{Re}(t_x t_y^*) = |t_x| \cdot |t_y| \cos\delta = 0, \tag{70}$$

where δ is the phase difference, defines the radii of circles containing the C-points. Note that, in weakly anisotropic NLCs, the phase difference δ can be approximated by the phase shift due to the difference in optical path of the ordinary and extraordinary waves, $\delta \approx \delta_e - \delta_o$, for the incidence angles up to 70°. Clearly, equation (70) implies that $\delta = \pi/2 + \pi k$, where $k = 0, 1 \ldots N - 1$ is the non-negative integer and N is the number of solutions. So, in the transverse projection plane, there are N circles with C-points. The radii of the circles ρ_k, $k = 0, 1 \ldots N - 1$, can be found by solving equation (70).

At $\rho = \rho_k$, it is not difficult to obtain the expressions for the amplitude of the components (69)

$$|\Psi_\nu(\rho_k, \phi)|^2 = 2|t|^2[1 + \cos 2\{\psi - \nu(-1)^k\alpha\}], \tag{71}$$

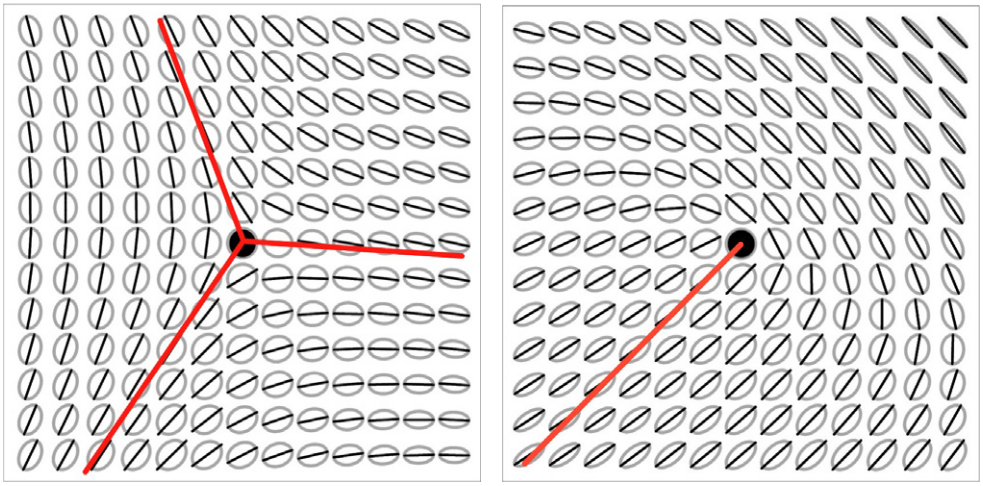

(a) Star: $I_C = -1/2$ and $N_C = 3$ (b) Lemon: $I_C = +1/2$ and $N_C = 1$

(c) Monstar: $I_C = +1/2$ and $N_C = 3$

Figure 2. Arrangement of the polarization ellipses around the C-points of three different types.

$$|t|^2 = |t_x|^2 + |t_y|^2, \qquad \tan\alpha = \frac{|t_y|}{|t_x|}. \tag{72}$$

From (71), it immediately follows that there are two pairs of C-points with the azimuthal angles given by

$$\phi_{\pm k}^{(\nu)} = \psi_p \pm \pi/2 + \nu(-1)^k\alpha \tag{73}$$

in each circle of radius ρ_k. The symmetric arrangement of the C-points (see also figure 3(a)) is a consequence of the symmetry relations

$$|\Psi_\nu(\rho,\psi)| = |\Psi_\nu(\rho,\pi+\psi)|, \qquad |\Psi_\nu(\rho,\psi)| = |\Psi_{-\nu}(\rho,\pi-\psi)| \tag{74}$$

for the amplitudes (69).

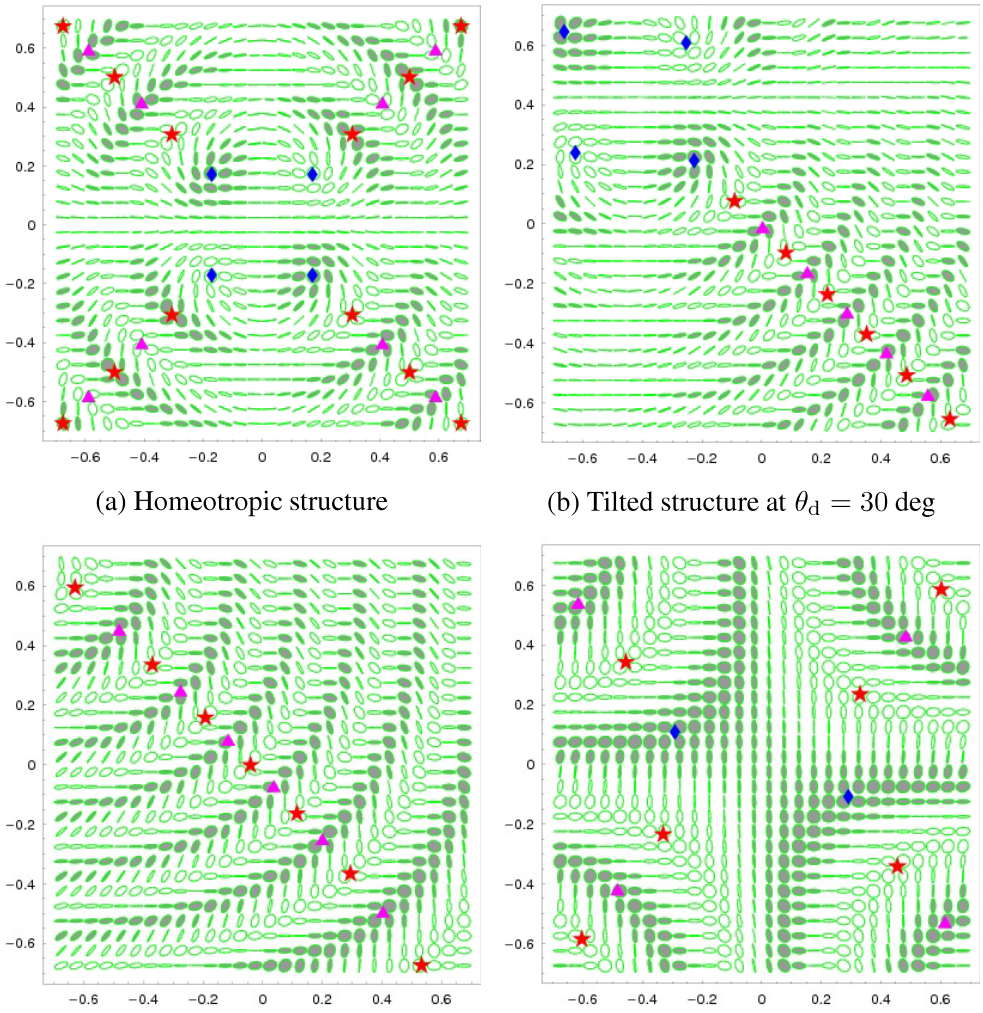

(a) Homeotropic structure

(b) Tilted structure at $\theta_{\rm d} = 30$ deg

(c) Tilted structure at $\theta_{\rm d} = 60$ deg

(d) Planar structure

Figure 3. The angular structure of polarization computed as the polarization ellipse field in the observation plane with the polar coordinates $\rho = \tan\theta_{\rm inc}$ and $\phi = \phi_{\rm inc}$. The incident light of wavelength 633 nm is linearly polarized with $\psi_p = 0$. Other parameters used in calculations are the cell thickness $d = 19$ μm, $\mu = \mu_{\rm m} = 1$, $n_{\rm m} = 1.5$, $n_e = n_1 = 1.71$ and $n_o = n_2 = n_3 = 1.527$ (5CB). The C-points of the lemon and the monstar types are marked by diamonds and triangles, respectively. Stars are used for the C-points of the star type. Left-handed and right-handed polarization is respectively indicated by open and filled ellipses.

We can now substitute equation (69) into the expression for the index (67) to derive the result

$$I_C = -\frac{1}{2}\,\mathrm{sign}[\partial_\rho R(\rho)]_{\rho=\rho_k} = \frac{(-1)^k}{2}, \tag{75}$$

where the second equality follows because R is an oscillating function of ρ and $R(0) > 0$.

Interestingly, equation (75) relates the index of C-points and derivatives of the transmission coefficients with respect to the incidence angle ($\partial_\rho f = \cos^2\theta_{\rm inc}\partial f/\partial\theta_{\rm inc}$). The index is thus

determined by the circle number k and alternates in sign starting from $I_C = +1/2$. So, the C-points in the vicinity of the origin at $\rho = \rho_0$ can either be lemons or monstars.

Now it is our task to formulate the criterion to distinguish between these two types. By using equation (69) we find the complex Stokes field (65) and the polarization azimuth (58)

$$\tilde{S} = 4\mathrm{e}^{2\mathrm{i}\phi} P, \qquad P = |t_x|^2 \cos^2\psi - |t_y|^2 \sin^2\psi - \mathrm{i}R \sin 2\psi, \tag{76}$$

$$2\phi_p = 2\phi + \arg P \tag{77}$$

for the homeotropic cell.

Our next step is to consider the first order term of the power series expansion of P in $\Delta x = \Delta r \cos\phi_r$ and $\Delta y = \Delta r \sin\phi_r$. The linear part of this expansion can be expressed in polar coordinates and, following the line of reasoning presented in [27], we derive the polynomial equation [44]

$$\tan 2(\phi_p - \phi) = \frac{2q}{1-q^2} = \frac{R_1}{|t|^2(q \mp \alpha_1)}, \tag{78}$$

$$R_1 \equiv (\rho\partial_\rho R)|_{\rho=\rho_k}, \qquad \alpha_1 \equiv (\rho\partial_\rho \alpha)|_{\rho=\rho_k} \tag{79}$$

in $q \equiv \tan(\phi_p - \phi) = \tan(\phi_r - \phi)$. The roots of (78) give the angles where $\phi_p = \phi_r$ (these lines are depicted in figure 2) and their number depends on the sign of the discriminant

$$D_L = (R_1/|t|^2 + 1)^2 + \alpha_1^2 - 1. \tag{80}$$

For $D_L < 0$, $N_C = 1$ and the point is of the lemon type. In the opposite case with $D_L > 0$, the C-points can either be stars or monstars depending on the index, $I_C = -1/2$ for stars and $I_C = +1/2$ for monstars.

As can be seen from equation (75), the derivative R_1 is positive if $I_C = -1/2$ and, as a result, $D_L > 0$. So, in agreement with the known result, our criterion leads to the conclusion that the C-points with $I_C = -1/2$ are always stars.

At $I_C = +1/2$, R_1 is negative and the point will be a monstar provided the gradients $|R_1|$ and $|\alpha_1|$ are sufficiently large. For example, the points where $R_1 < -2|t|^2$ are monstars. As is illustrated in figure 3(a), in sufficiently thick cells, the C-points with $k \geqslant 2$ and $I_C = 1/2$ are monstars, whereas the C-points in the circle of the smallest radius ($k = 0$) are lemons.

More generally, monstars will be the dominating type in regions of pronounced dependence of the transmission coefficients on the incidence angle. By contrast, a mechanism suppressing strong inhomogeneity may drastically increase the fraction of lemons. For example, in liquid crystals, strong director deformations (and large gradients) are inhibited due to the elastic energy costs and, thus, disclinations of the monstar type are generally unstable [1].

For the homeotropic configuration, the condition (68) can be simplified, giving the equation

$$\mathrm{Im}(t_x t_y^*) \sin 2\psi = 0 \tag{81}$$

that describes the L-lines. From (81) there are two straight lines of linear polarization: $\phi = \psi_p$ and $\phi = \psi_p + \pi/2$, where the polarization vectors of incident and transmitted waves are parallel, $\phi_p = \psi_p$.

Other L-lines are circles separating the circles of C-points. The radii of the circles, $\rho_k^{(L)}$, can be found as the solutions to the equation $\delta = \pi k$ with $k = 1, \ldots, N-1$. When k is even and $|t_x| \approx |t_y|$, from equation (77) it can be concluded that, similar to the straight L-lines, $\phi_p \approx \psi_p$. If k is odd, the polarization vector rotates with the azimuthal angle of the incidence plane and $\phi_p \approx \psi_p + 2\phi$. These can also be seen in figure 3(a).

3.3. Director tilt and biaxiality induced effects

The analytical results presented in the previous section completely characterize the transmission angular pattern of the light polarization for the homeotropic orientational structure in terms of the polarization singularities. In figure 3(a), this polarization resolved conoscopic pattern is depicted as the field of polarization ellipses in the projection plane where $x = \tan\theta_{\rm inc}\cos\phi_{\rm inc}$ and $y = \tan\theta_{\rm inc}\sin\phi_{\rm inc}$.

Referring to figure 3(a) (see also equation (73)), when $|t_x| \approx |t_y|$ and $\alpha \approx \pi/4$, the C-points are arranged in chains formed by four rays along which they alternate in sign of the handedness and of the index. The symmetry of the chain structure can be deduced from the symmetry relations (74).

In particular, the structure is invariant with respect to the operation of reflection: $\psi \to -\psi$ and $\nu \to -\nu$. It additionally possesses a symmetry centre located at the origin and associated with the transformation of inversion: $\phi \to \phi + \pi$. Clearly, each of the two straight L-lines, $\phi = \psi_p$ and $\phi = \psi_p + \pi/2$, is a symmetry axis and the symmetry centre is also the centre of the L-circles.

Algebraically, the symmetry properties of the polarization pattern follow because the transmission matrix for the homeotropic cell (51) is diagonal and the transmission coefficients, t_x and t_y, are independent of the azimuthal angle of the incidence plane, $\phi = \phi_{\rm inc}$. For tilted director configurations with $0 < \theta_{\rm d} < \pi/2$, this is no longer the case.

In this case, the transmission matrix (45) is non-diagonal and its elements depend on $\phi_{\rm d} - \phi$. Generally, there are two types of the azimuthal angle dependent terms: (a) the terms proportional to $\cos 2(\phi_{\rm d} - \phi)$ and (b) the inversion symmetry breaking terms proportional to either $\sin(\phi_{\rm d} - \phi)$ or $\cos(\phi_{\rm d} - \phi)$.

In figure 3, we show what happens when the tilt angle $\theta_{\rm d}$ varies from $\theta_{\rm d} = 0$ to $\pi/2$, so that the orientational structure changes from the homeotropic configuration to the planar one. From figure 3(b) it is seen that, at small incidence angles, the symmetry breaking terms result in the shift of the symmetry centre. When the incidence angle $\theta_{\rm d}$ increases further, the centre of symmetry eventually leaves the region specified by the aperture, leading to the single-chain structure of the C-points shown in figure 3(c).

In the case of the planar structure with $d_z = 0$ ($\theta_{\rm d} = \pi/2$), it is not difficult to see that the terms dependent on the azimuthal angle ϕ are proportional either to d_y^2 or to d_x^2. So, similar to the homeotropic cell, the origin is the symmetry centre for the polarization pattern of light passed through the planar cell. Figure 3(d) demonstrates that, in contrast to the homeotropic structure, where the polarization field is of the elliptic type (see figure 3(a)), the angular pattern of polarization is of the hyperbolic type for the planar structure.

The results computed for weakly biaxial orientational configurations are presented in figure 4. In these calculations, the Euler angles, $\phi_{\rm d}$ and $\gamma_{\rm d}$, that specify orientation of the principal axes (2), are taken to be zero and $\pi/4$, respectively. In figure 4(a), similar to the homeotropic cell, the tilt angle $\theta_{\rm d}$ is zero, whereas the polarization pattern for the tilted biaxial structure (see figure 4(b)) was calculated as $\theta_{\rm d} = 10^\circ$. From the patterns plotted in figures 4(a) and (b) it is clear that biaxiality induces additional deformations of the polarization ellipse field as compared to the case of uniaxially anisotropic cells.

4. Discussion and conclusions

In this paper we have studied the polarization resolved angular patterns of light transmitted through uniformly anisotropic NLC cells. Such patterns can be considered as the polarization structure underlying the conoscopic images measured in experiments with two crossed polarizers.

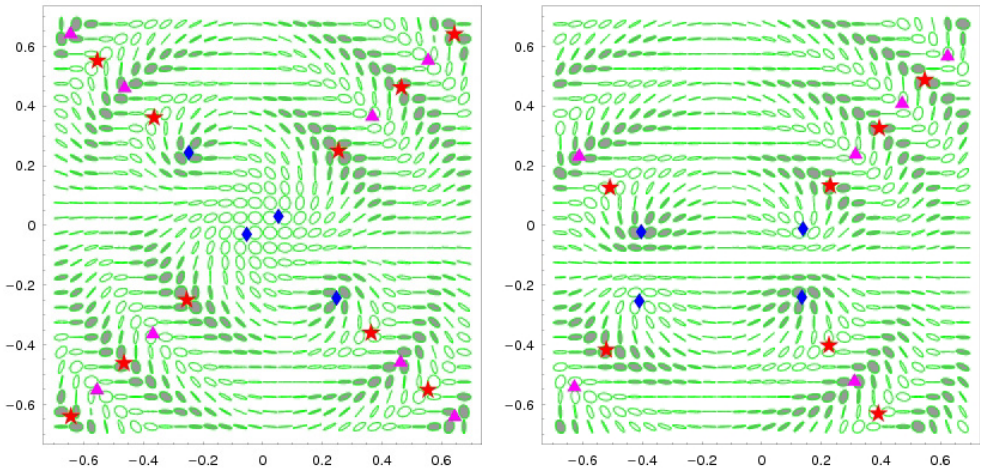

(a) Biaxial structure at $\theta_{\mathrm{d}} = 0$ deg. (b) Biaxial structure at $\theta_{\mathrm{d}} = 10$ deg.

Figure 4. The angular structure of polarization computed as the polarization ellipse field in the observation plane with the polar coordinates $\rho = \tan\theta_{\mathrm{inc}}$ and $\phi = \phi_{\mathrm{inc}}$. The incident light of wavelength 633 nm is linearly polarized with $\psi_p = 0$. Other parameters used in calculations are the cell thickness $d = 19\ \mu$m, $\mu = 1$, $\gamma_{\mathrm{d}} = 45°$, $n_1 = 1.71$, $n_2 = 1.52$ and $n_3 = 1.53$. The C-points of the lemon and the monstar types are marked by diamonds and triangles, respectively. Stars are used for the C-points of the star type. Left-handed and right-handed polarization is respectively indicated by open and filled ellipses.

Experimentally, this structure can be investigated using a suitably modified method of the Stokes polarimetry designed for accurate measurements of the Stokes parameters (typical experimental set-ups are described, e.g., in [25, 30]). The predictions of our theory for the homeotropic cell was successfully compared with the polarization patterns experimentally obtained by the group of experimentalists at the Institute of Physics of NASU (Kyiv, Ukraine). This is demonstrated in figure 5. These results will be detailed in a separate joint publication [51].

The exact solution to the transmission (reflection) problem for the uniformly anisotropic cell was derived in section 2 by using the 4×4 matrix formalism in combination with the orthogonality relations. We deduced the relation linking the operator of evolution and the transmission (reflection) matrix (see (19) and (20)). Then the basis of eigenwaves was used to construct the operator of evolution (41). After simplifying algebraic rearrangements made with the help of the orthogonality relations (15), the final result (see (45) and (46)) was expressed in terms of 2×2 matrices.

For the case of one interfacial (reflecting) surface, the explicit formulas in the 2×2 matrix form were previously derived in [45, 46]. Algorithms and useful approximations for inhomogeneous z-stratified anisotropic media were suggested in more recent papers [47–50]. For our purposes, however, it is sufficient to have the exact expressions in the compact convenient form that emphasize the symmetry properties of the transmission matrix and enormously simplify numerical calculations. Leaving aside an extended discussion of generalizations and approximation schemes, we just note that relations (19) and (20) can be combined with approximations for the operator of evolution constructed by applying expression (41) for homogeneous sublayers.

The analytical results were applied to characterize the polarization resolved angular patterns in terms of the polarization singularities such as C-points and L-lines. The case of

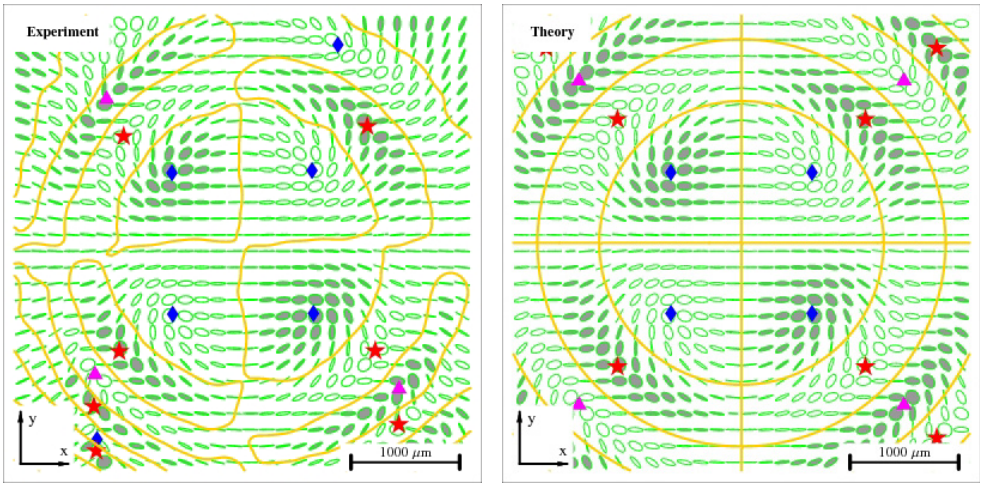

(a) Experiment (b) Theory

Figure 5. (a) The polarization resolved angular pattern measured in the homeotropic cell of thickness $d = 110$ μm filled with the nematic liquid crystal mixture E7 ($n_e = 1.76$ and $n_o = 1.52$). The incident light of the wavelength 633 nm (He–Ne laser) is linearly polarized at $\psi_p = 0$. (b) The pattern computed using the transmission matrix (51). L-lines are shown as solid lines.

the homeotropic director configuration was analysed in detail. We found that the singularities are symmetrically arranged and deduced the simple formula for the index of C-points. We have also formulated the quantitative criterion to determine the type of the C-points.

The C-points are shown to form chains along which they alternate in sign of the handedness and the index, I_C. At $I_C = -1/2$, all the C-points are stars, whereas the C-points with $I_C = +1/2$ can either be lemons or monstars depending on how strong the dependence of the transmission coefficients on the incidence angle is. In sufficiently thick NLC layers ($d > 10$ μm for 5CB), the C-points of the lemon type are found to be located in the immediate vicinity of the origin.

The patterns for the tilted, planar and weakly biaxial configurations were computed numerically and presented as the polarization ellipse fields. The primary goal of these calculations is to demonstrate the effects of director orientation and biaxiality on the polarization resolved angular patterns. At this stage we can only hope that these effects can be used to develop an improved experimental technique for detecting the peculiarities of liquid crystal orientational structures. But our results can be regarded as a first step in this direction.

The applicability of our results is not restricted to the case of nematic cells that were discussed as technologically important materials. In our considerations, a nematic liquid crystal can be easily changed for another uniformly anisotropic medium.

Our concluding remark concerns the effects related to the polarization state of the incident light. For definiteness, in sections 3.2 and 3.3, this wave was assumed to be linearly polarized. More generally, the ellipticity and the polarization azimuth of the incident wave can be regarded as additional governing parameters that may have a profound effect on the polarization angular patterns.

For example, it can be shown that, for the homeotropic cell, variations of the ellipticity parameter of the incident wave induce transformations of the angular pattern involving creation and annihilation of the C-points. In the limiting case where the incident light is circularly polarized, the angular pattern is characterized by the only C-point located at the origin.

The effects of the incident wave polarization can also be studied in terms of generalized polarization patterns in differently parametrized planes. We shall expand on this subject in our subsequent publication [51].

Acknowledgments

This work was partially supported by CERG grant no 612406. The author is grateful to Professor V G Chigrinov and Professor H-S Kwok (Hong Kong University of Science and Technology) for useful conversations and hospitality during his visits to HK. Numerous discussions with Professor M S Soskin (Institute of Physics of NASU, Kyiv, Ukraine) are gratefully acknowledged. We also thank I A Buinyi for assistance with computer graphics and R G Vovk for making the measurements.

References

[1] de Gennes P G and Prost J 1993 *The Physics of Liquid Crystals* (Oxford: Clarendon)
[2] Yeh P and Gu C 1999 *Optics of Liquid Crystal Displays* (Singapore: Wiley)
[3] Chigrinov V G 1999 *Liquid Crystal Devices: Physics and Applications* (Boston, MA: Artech House)
[4] Baur G, Wittwer V and Berreman D W 1976 *Phys. Lett.* **56** 142
[5] Yu L J and Saupe A 1980 *Phys. Rev. Lett.* **45** 1000
[6] Madsen L A, Dingemans T J, Nakata M and Samulski E T 2004 *Phys. Rev. Lett.* **92** 145505
[7] Komitov L, Hauk G and Koswig H D 1984 *Cryst. Res. Technol.* **19** 253
[8] Brett L H and Winter H H 2001 *Appl. Opt.* **40** 2089
[9] Gorecka E, Chandani A D L, Ouchi Y, Takezoe H and Fukuda A 1990 *Japan. J. Appl. Phys.* **29** 131
[10] Suwa S, Hoshi H, Takanishi Y, Ishikawa K, Takezoe H and Zeks B 2003 *Japan. J. Appl. Phys.* **42** 1335
[11] Nastishin Y A, Dovgyi O B and Vlokh O G 2001 *Ukr. J. Phys. Opt.* **2** 98
[12] Nye J F 1983 *Proc. R. Soc.* A **389** 279
[13] Nye J F and Hajnal J V 1987 *Proc. R. Soc.* A **409** 21
[14] Nye J F 1999 *Natural Focusing and Fine Structure of Light: Caustics and Wave Dislocations* (Bristol: IOP Publishing)
[15] Hajnal J V 1987 *Proc. R. Soc.* A **414** 433
[16] Hajnal J V 1987 *Proc. R. Soc.* A **414** 447
[17] Hajnal J V 1990 *Proc. R. Soc.* A **430** 413
[18] Freund I and Shvartsman N 1994 *Phys. Rev.* A **50** 5164
[19] Freund I, Mokhun A I, Soskin M S, Angelsky O V and Mokhun I I 2002 *Opt. Lett.* **27** 545
[20] Berry M V and Dennis M R 2000 *Proc. R. Soc.* A **456** 2059
[21] Berry M V and Dennis M R 2001 *Proc. R. Soc.* A **457** 141
[22] Konukhov A I and Melnikov A L 2001 *J. Opt. B: Quantum Semiclass. Opt.* **3** S139
[23] Freund I 2002 *Opt. Commun.* **201** 251
[24] Freund I, Soskin M S and Mokhun A I 2002 *Opt. Commun.* **208** 223
[25] Soskin M S, Denisenko V and Freund I 2003 *Opt. Lett.* **28** 1475
[26] Mokhun A I, Soskin M S and Freund I 2002 *Opt. Lett.* **27** 995
[27] Dennis M R 2002 *Opt. Commun.* **213** 201
[28] Berry M V and Dennis M R 2003 *Proc. R. Soc.* A **459** 1261
[29] Berry M V 2005 *Proc. R. Soc.* A **461** 2071
[30] Flossmann F, Schwarz U T and Dennis M R 2005 *Phys. Rev. Lett.* **95** 253901
[31] Luckhurst G R 2001 *Thin Solid Films* **393** 40
[32] Luckhurst G R 2004 *Nature* **430** 413
[33] Severing K and Saalwächter K 2004 *Phys. Rev. Lett.* **92** 125501
[34] Smith D O 1965 *Opt. Acta* **12** 13
[35] Berreman D W 1972 *J. Opt. Soc. Am.* **62** 502
[36] Oldano C 1989 *Phys. Rev.* A **40** 6014
[37] Yakovlev D A 1998 *Opt. Spectrosc.* **84** 923
[38] Born M and Wolf E 1980 *Principles of Optics* 2nd edn (Oxford: Pergamon)
[39] Yariv A and Yeh P 1984 *Optical Waves in Crystals* (New York: Wiley–Interscience)

[40] Azzam R M A and Bashara N M (ed) 1977 *Ellipsometry and Polarized Light* (Amsterdam: North-Holland)
[41] Mermin N D 1979 *Rev. Mod. Phys.* **51** 591
[42] Berry M V 2004 *J. Opt. A: Pure Appl. Opt.* **6** 675
[43] Berry M V and Hannay J H 1977 *J. Phys. A: Math. Gen.* **10** 1809
[44] Kiselev A D 2006 Polarization resolved angular patterns in nematic liquid crystal cells *Preprint* physics/0612114
[45] Lekner J 1991 *J. Phys.: Condens. Matter* **3** 6121
[46] Lekner J 1992 *J. Phys.: Condens. Matter* **4** 1387
[47] Yakovlev D A 1999 *Opt. Spectrosc.* **87** 990
[48] Yakovlev D A 2003 *Opt. Spectrosc.* **94** 600
[49] Yakovlev D A 2003 *Opt. Spectrosc.* **95** 944
[50] Palto S P 2001 *JETP* **92** 552
[51] Kiselev A D, Soskin M S, Buinyi I A and Vovk R G 2007 in preparation